



Accurate and simple measurement of power generation efficiency and figure of merit of thermoelectric modules based on optical heating and non-contact temperature detection methods

Naoki Nakamura, Fuyuki Ando, Ken-ichi Uchida, Masayuki Murata, Abdulkareem Alasli & Hosei Nagano

To cite this article: Naoki Nakamura, Fuyuki Ando, Ken-ichi Uchida, Masayuki Murata, Abdulkareem Alasli & Hosei Nagano (2025) Accurate and simple measurement of power generation efficiency and figure of merit of thermoelectric modules based on optical heating and non-contact temperature detection methods, Science and Technology of Advanced Materials, 26:1, 2551485, DOI: [10.1080/14686996.2025.2551485](https://doi.org/10.1080/14686996.2025.2551485)

To link to this article: <https://doi.org/10.1080/14686996.2025.2551485>



© 2025 The Author(s). Published by National Institute for Materials Science in partnership with Taylor & Francis Group.



Published online: 10 Sep 2025.



[Submit your article to this journal](#)



Article views: 467



[View related articles](#)



[View Crossmark data](#)

Accurate and simple measurement of power generation efficiency and figure of merit of thermoelectric modules based on optical heating and non-contact temperature detection methods

Naoki Nakamura^a, Fuyuki Ando^b, Ken-ichi Uchida^{b,c}, Masayuki Murata^d, Abdulkareem Alasli^a and Hosei Nagano^a

^aDepartment of Mechanical Systems Engineering, Nagoya University, Nagoya, Japan;

^bResearch Center for Magnetic and Spintronic Materials, National Institute for Materials Science (NIMS), Tsukuba, Japan;

^cDepartment of Advanced Materials Science, The University of Tokyo, Kashiwa, Japan;

^dResearch Institute for Energy Efficient Technologies, National Institute of Advanced Industrial Science and Technology (AIST), Tsukuba, Japan

ABSTRACT

In this study, we propose an accurate, simple, and versatile measurement method for power generation efficiency and device figure of merit ZT of thermoelectric devices. Toward the energy harvesting applications of thermoelectric generators, the performance characterization under low heat inflow and temperature difference is crucial. However, when the conventional solid-state heat flow meter is used, the uncertainty of power generation performance increases as heat input decreases. We have solved these problems by using a laser for heat input, improving the simplicity and accuracy of power generation efficiency measurements, especially at low heat flow. The direct and non-contact measurement of the temperature difference by using a thermography allowed us to determine ZT as well as power generation efficiency. The obtained mean power generation efficiency and ZT values are consistent with the values obtained by the conventional method within the error range, thereby validating the reliability of the proposed method. The relative uncertainties of the efficiency and ZT were estimated to be less than 3% and 12% for our method, respectively, whereas those were 19% and 24% in situations where the temperature difference was less than 6 K for the conventional method.

ARTICLE HISTORY

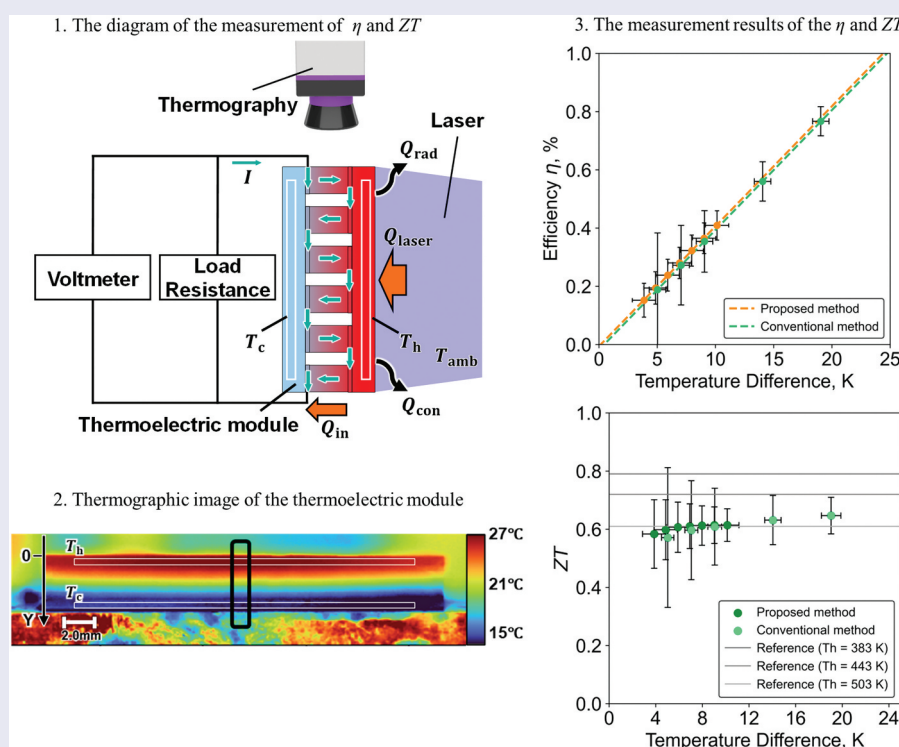
Received 31 March 2025

Accepted 19 August 2025

Revised 11 August 2025





KEYWORDS

Thermoelectric figure of merit; thermoelectric generator; laser heating; thermography



IMPACT STATEMENT

A fully non-contact method was proposed to evaluate η and ZT of thermoelectric devices, achieving uncertainties of less than 3% and 12%, respectively, using laser heating and thermographic temperature measurement.

CONTACT Hosei Nagano  nagano@mech.nagoya-u.ac.jp  Department of Mechanical Systems Engineering, Nagoya University, Furo-cho, Chikusa-ku, Nagoya, Aichi 464-8603, Japan; Fuyuki Ando  ANDO.Fuyuki@nims.go.jp  Research Center for Magnetic and Spintronic Materials, National Institute for Materials Science (NIMS), 1-2-1 Sengen, Tsukuba, Ibaraki 305-0047, Japan

© 2025 The Author(s). Published by National Institute for Materials Science in partnership with Taylor & Francis Group.

This is an Open Access article distributed under the terms of the Creative Commons Attribution License (<http://creativecommons.org/licenses/by/4.0/>), which permits unrestricted use, distribution, and reproduction in any medium, provided the original work is properly cited. The terms on which this article has been published allow the posting of the Accepted Manuscript in a repository by the author(s) or with their consent.

1. Introduction

Due to rising energy costs, the depletion of fossil fuel resources and the increasing severity of environmental issues, energy systems are undergoing a significant transition [1]. Thermoelectric generator (TEG) can directly convert heat into electricity and has long been attracting attention as an environmentally friendly energy conversion method [2–5]. TEGs have been widely developed for application in automobiles [6,7], wearable devices [8,9], photovoltaic systems [10–12], and industrial waste heat power generation [13,14] due to their advantages of frictionless operation, high reliability and stability, and low installation and maintenance costs [15–18]. In recent years, a combined Internet of Things (IoT)-thermoelectric system has also been considered, in which thermoelectric devices are used to generate electricity from factory waste heat to provide an independent power source for IoT devices. As TEGs are operated and systematized in these various fields, it is becoming more and more important to ensure stable power output. In particular, accurate performance evaluation at low heat input is increasingly required in the field of energy harvesting [19,20].

The performance of thermoelectric devices is typically characterized in terms of the following two important parameters. One is the power generation efficiency η , which indicates how much output power is obtained from the input heat flow. The other is the device thermoelectric figure of merit ZT , which determines the thermoelectric performance of the device itself [21,22]. Proper evaluation of η requires simultaneous measurement of input heat flow Q_{in} and output power P_{out} according to the following equation:

$$\eta = \frac{P_{out}}{Q_{in}} \quad (1)$$

The conventional method to determine Q_{in} is a steady-state heat flow method using a solid-state heat flow meter (HFM) [23–26]. In this method, Q_{in} can be calculated using the 1D Fourier's law from the temperature difference ΔT_M within HFM. P_{out} is simultaneously measured by a four terminal method, followed by the calculation of η . However, this method has several limitations. Firstly, we need to arrange the area of HFM with that of the thermoelectric device to realize the one-dimensional heat transport. Secondly, as ΔT_M within HFM becomes smaller, the uncertainty of the absolute temperature causes a larger error in the estimated Q_{in} . Meanwhile, ZT is mainly used to compare the thermoelectric performance of various devices without the effect of Carnot efficiency as follows:

$$ZT = \left(\frac{T_h - T_c(1 - \eta_{max})}{T_h(1 - \eta_{max}) - T_c} \right)^2 - 1 \quad (2)$$

Although ZT is the common indicator in the field of thermoelectrics, the accurate measurement especially at low Q_{in} has been difficult mainly due to the uncertainty of ΔT_M within HFM and hence Q_{in} .

This study presents a new method to characterize thermoelectric performance using a laser and a thermography. Because we directly estimate Q_{in} from an injected laser power [27–32] instead of a solid-state heat flow sensor, the measurement error is significantly reduced even in the low Q_{in} condition. This enables an accurate measurement of η over a wide range of Q_{in} , which has been difficult for the conventional method. In addition, the area of the laser injection can be flexibly changed according to the thermoelectric modules with various sizes and shapes. Furthermore, the proposed method can simultaneously and precisely measure ZT in low heat input by directly measuring the temperature distribution in the module. We applied this method to a commercially available thermoelectric device with the known η and ZT and compared the results with those obtained by the conventional method using HFM. As a result, our data shows a quantitative agreement with a specification of the device [33] and much lower error in low heat input than that by the conventional method. The proposed method will contribute to the acceleration of energy harvesting applications of thermoelectric devices.

2. Measurement principles and setup

2.1. Measurement principles

Figure 1 shows the schematic of our measurement principle. Q_{in} is estimated by measuring the heat absorbed from the laser on the heating surface and subtracting the heat loss from the surface. The relationship between Q_{in} and the laser output Q_{laser} can be described by Equation (3), which incorporates the absorptance α (using black coating) of the device surface and the convective heat loss Q_{con} and radiative heat loss Q_{rad} to the surroundings:

$$Q_{in} = \alpha Q_{laser} - Q_{con} - Q_{rad} \quad (3)$$

Q_{con} and Q_{rad} are given by

$$Q_{con} = hA(T_h - T_{amb}) \quad (4)$$

$$Q_{rad} = \varepsilon \sigma A(T_h^4 - T_{amb}^4) \quad (5)$$

respectively, where T_{amb} is the ambient temperature, $h = 10$ the heat transfer coefficient between the device surface and air, A the area of the device surface, and ε the emissivity of the surface. P_{out} is measured from Equation (6) by attaching a variable load resistance R_{out} :

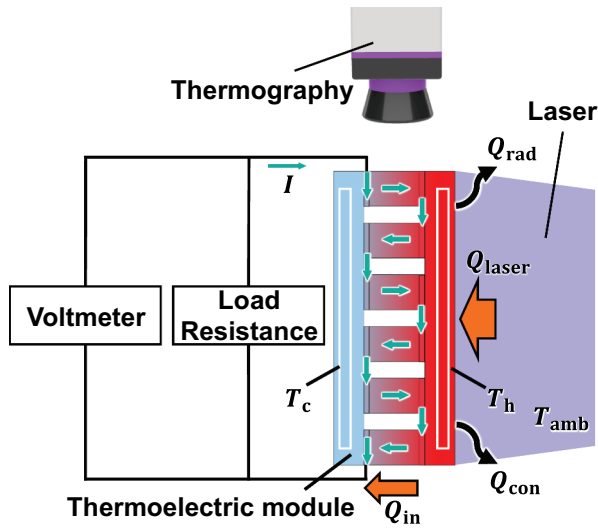


Figure 1. The diagram of the simultaneous measurement of the power generation efficiency η and device figure of merit ZT .

$$P_{out} = IV = \frac{V^2}{R_{in} + R_{out}} \quad (6)$$

where I , V , and R_{in} are the current, voltage, and internal resistance of the thermoelectric device, respectively. The value of R_{out} is varied, and the maximum output power P_{max} is calculated from the load resistance dependence. Then, since the value of Q_{in} is a constant value, we can calculate the maximum efficiency from Q_{in} and P_{max} .

$$\eta_{max} = \frac{P_{max}}{Q_{in}} \quad (7)$$

ZT can be derived from the one-dimensional heat conduction equation and the electric circuit theory, and the equation is expressed as in Equation (7) using the value of maximum power generation efficiency η_{max} and T_h and T_c [24]

2.2. Measurement apparatus

Figure 2 shows a schematic diagram of the apparatus for this measurement. The apparatus consists mainly of a diode laser, thermography, variable resistor, voltmeter, chiller, cold plate, and PC. The diode laser with a wavelength of 455 nm was used for the thermal input to the thermoelectric device. The laser intensity value was set to be the actual intensity output from the laser as measured with a power meter, and the input shape of the laser was adjusted to match the shape of the module. A mode mixer was also used to ensure uniform heating within the surface. T_h and T_c were determined by observing the side surface of the device with the thermography, sending the data to the PC, and then averaging the temperatures in the areas of aluminum oxide plates for the hot and cold sides, respectively. The cold side of the

device was bonded to the cold plate, and the temperature on the cold side was controlled by the chiller. Then, the laser intensity to heat the module surface was set by the PC, and heat input was started. The laser-heated surfaces of the module and the observation surfaces of the thermography were coated with black paint (JAPAN SENSOR JSC-3). In this measurement, the optical absorbance at the laser wavelength (455 nm) and the emissivity near room temperature (corresponding to wavelengths around 10 μm) were set to 0.983 and 0.94, respectively, using the experimentally measured value obtained with the UV-Vis spectrophotometer (V-670, JASCO) and the catalog value [34]. After T_h and T_c were stabilized within $\pm 0.1^\circ\text{C}$, the value of the load resistance was varied to find the maximum P_{out} . Q_{in} was calculated from Equations (3)–(5) by substituting the values of T_h and T_c . By repeating this process with different laser intensities, the η and ZT values at various temperature differences $\Delta T = T_h - T_c$ were calculated. This thermography is calibrated using a black plate with the emissivity of 0.94 before each measurement [35]. In addition, the temperature measurement is calibrated periodically by inter-measurement with a thermocouple coated with black paint.

3. Measurement

3.1. Verification sample and measurements conditions

The module used in this study is the SINGLE-STAGE THERMOELECTRIC GENERATOR TG12–2.5, and its specifications are summarized in Table 1 [33]. It should be noted that the ZT value varies depending on the measured temperature range: 0.61, 0.72 and 0.79 at $T_h = 110, 170$, and 230°C , respectively, with the fixed

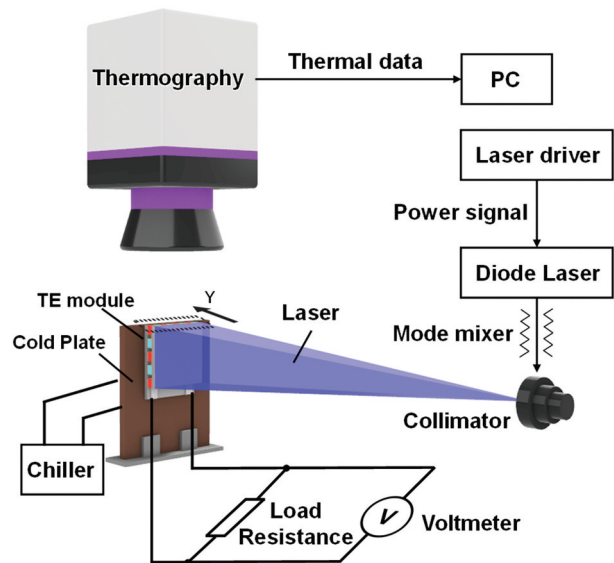


Figure 2. Schematic diagram of the measurement apparatus.

Table 1. Specifications of sample module [33]. The load resistance for optimum η and ZT values are measured in $T_h = 110, 170, 230^\circ\text{C}$ and $T_c = 50^\circ\text{C}$.

Ceramic Area	Module Height	AC Resistance	Load Resistance for Optimum η	ZT
30 mm \times 30 mm	3.94 mm	4.47–5.69 Ω	10.47, 9.68, 8.75 Ω	0.61, 0.72, 0.79

$T_c = 50^\circ\text{C}$, indicating the large temperature dependence of the thermoelectric properties for the constituent thermoelectric legs.

The experimental conditions were as follows: the cold plate temperature was set at 15°C and the laser power was varied from 1500 mW to 4500 mW in increments of 500 mW. Measurements were conducted in the atmosphere. An average value was taken from five measurements at each laser power setting.

3.2. Temperature measurements

Figure 3(a) shows an example of the thermography image data at the laser power of 4500 mW, where T_h and T_c are defined around the central area of aluminum oxide plates to eliminate the influence of heat loss near the edges. The standard deviation of the temperature was less than 0.4°C in all measurement conditions. Figure 3(b) showed the averaged line scan data in the direction of heat flow in the black area marked in Figure 3(a). Figure 3(c) shows ΔT

proportional to ΔT , and the maximum P_{out} increases in proportion to the square of ΔT with neglecting the temperature dependence of thermoelectric properties of the constituent thermoelectric legs.

4. Error analysis and experimental results

4.1. Error analysis

We describe the error analysis procedure in detail. The relative uncertainty of Q_{in} takes into account the uncertainty in Q_{laser} , α , A , T_h and variations in the heat transfer coefficient h , which ranges from 7 to 15 $\text{W}/\text{m}^2 \text{K}$ under natural air-cooled environment. Meanwhile, the relative uncertainty of the P_{out} includes the variable resistance value and the uncertainty in the V measurement. From the law of error propagation, the relative uncertainties are, respectively, expressed by the following equations:

$$\frac{u_{\text{proposed}}(Q_{\text{in}})}{Q_{\text{in}}} = \sqrt{\left(\frac{\partial Q_{\text{in}}}{\partial \alpha} \delta \alpha\right)^2 + \left(\frac{\partial Q_{\text{in}}}{\partial Q_{\text{laser}}} \delta Q_{\text{laser}}\right)^2 + \left(\frac{\partial Q_{\text{in}}}{\partial h} \delta h\right)^2 + \left(\frac{\partial Q_{\text{in}}}{\partial A} \delta A\right)^2 + \left(\frac{\partial Q_{\text{in}}}{\partial \varepsilon} \delta \varepsilon\right)^2 + \left(\frac{\partial Q_{\text{in}}}{\partial T_h} \delta T_h\right)^2 + \left(\frac{\partial Q_{\text{in}}}{\partial T_{\text{amb}}} \delta T_{\text{amb}}\right)^2} \quad (8)$$

dependence of Q_{in} calculated using the above data. As shown in Figure 3(a, b), the surface was homogeneously heated realizing a one-dimensional heat transport in Y-direction.

3.3. Output power measurement

We characterized the maximum P_{out} with varying R_{out} under the application of Q_{in} . Firstly, the DC internal resistance of the thermoelectric device R_{in} at each condition was calculated from the slope of the measured I - V curve, where I is tuned by changing R_{out} . The R_{in} value calculated from Figure 4(a) is 4.81Ω , which is consistent with the catalog reference value in Table 1. Figure 4(b) shows the I dependence of $P_{\text{out}} (= IV)$ at various Q_{in} values, where R_{out} for the maximum output condition at 1500 mW was 8.52Ω , which is also confirmed to be close to the reference value of optimum η . Based on these data, Figure 4(c, d) show the open-circuit voltage and maximum P_{out} versus ΔT at each laser output. Here, since all the measurements were performed around room temperature, the open-circuit voltage is

$$\frac{u_{\text{proposed}}(P_{\text{out}})}{P_{\text{out}}} = \sqrt{\left(\frac{\partial P_{\text{out}}}{\partial R_{\text{out}}} \delta R_{\text{out}}\right)^2 + \left(\frac{\partial P_{\text{out}}}{\partial V} \delta V\right)^2} \quad (9)$$

Based on these equations, the relative uncertainty of η is given by

$$\frac{u_{\text{proposed}}(\eta)}{\eta} = \sqrt{\left(\frac{\partial \eta}{\partial Q_{\text{in}}} \delta Q_{\text{in}}\right)^2 + \left(\frac{\partial \eta}{\partial P_{\text{out}}} \delta P_{\text{out}}\right)^2} \quad (10)$$

In the steady-state heat flow method using HFM (hereinafter, referred to as the conventional method) [36], Q_{in} is expressed as

$$Q_{\text{in}} = Q_{\text{out}} + P_{\text{out}} \quad (11)$$

$$Q_{\text{out}} = kA(T_u - T_b) \quad (12)$$

where Q_{out} represents the heat flow from the cold side of the module, k is the thermal conductivity of HFM, and T_u , T_b are the temperatures at the hot and cold

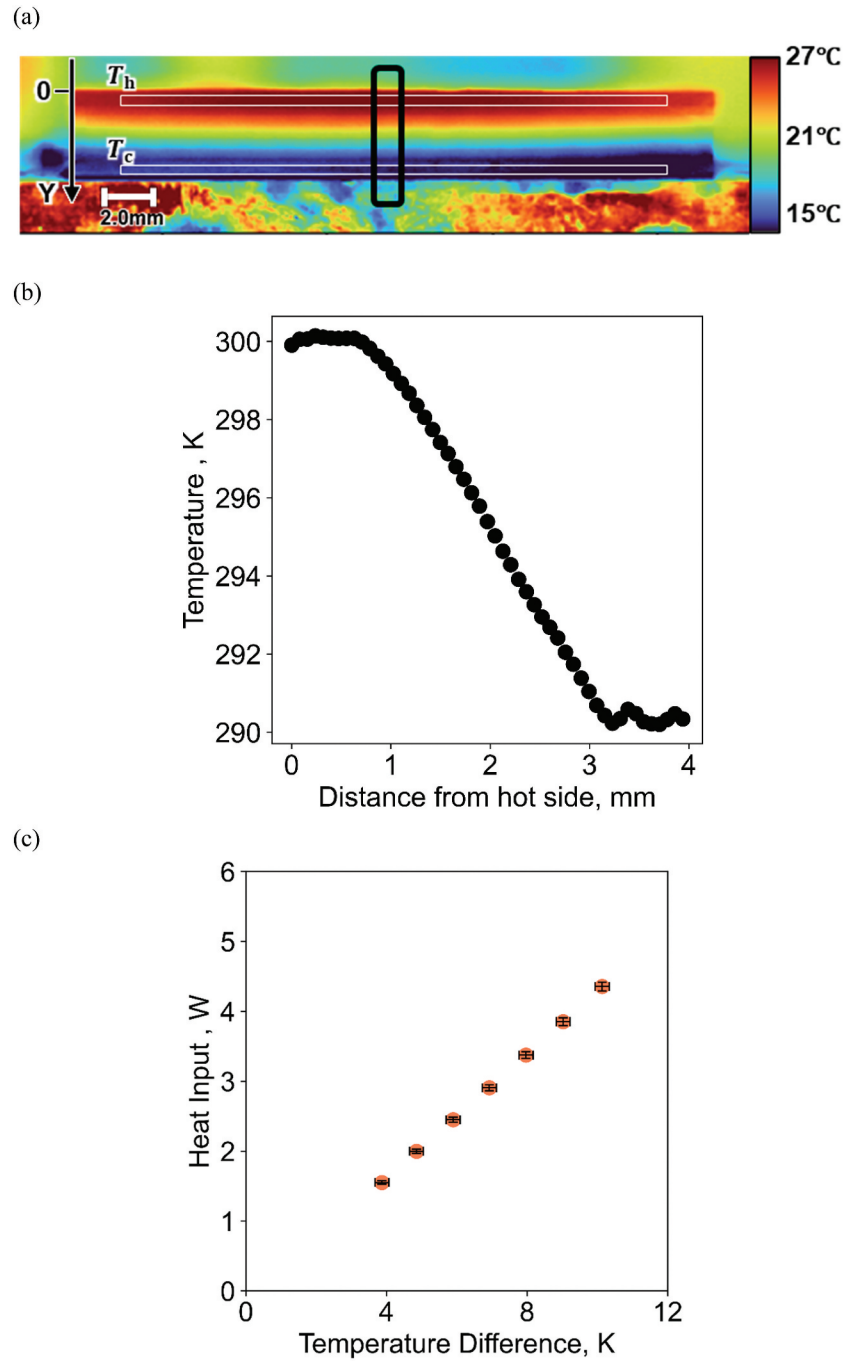


Figure 3. (a) Thermographic image of the side surface of the thermoelectric module when 4500 mW is applied, (b) line scan data in the direction of heat flow in the black area marked in (a), (c) Q_{in} as a function of T .

side temperatures in HFM. Therefore, the relative uncertainty of η for the conventional method is expressed as:

$$\frac{u_{conventional}(Q_{in})}{Q_{in}} = \sqrt{\left(\frac{\partial Q_{in}}{\partial k} \delta k\right)^2 + \left(\frac{\partial Q_{in}}{\partial A} \delta A\right)^2 + \left(\frac{\partial Q_{in}}{\partial T_u} \delta T_u\right)^2 + \left(\frac{\partial Q_{in}}{\partial T_b} \delta T_b\right)^2 + \left(\frac{\partial Q_{in}}{\partial P_{out}} \delta P_{out}\right)^2} \quad (13)$$

$$\frac{u_{conventional}(P_{out})}{P_{out}} = \sqrt{\left(\frac{\partial P_{out}}{\partial R_{out}} \delta R_{out}\right)^2 + \left(\frac{\partial P_{out}}{\partial V} \delta V\right)^2} \quad (14)$$

It should be noted that it is assumed that the uncertainty due to P_{out} is negligibly small in the conventional method. The relative uncertainty of ZT is calculated from the following equation:

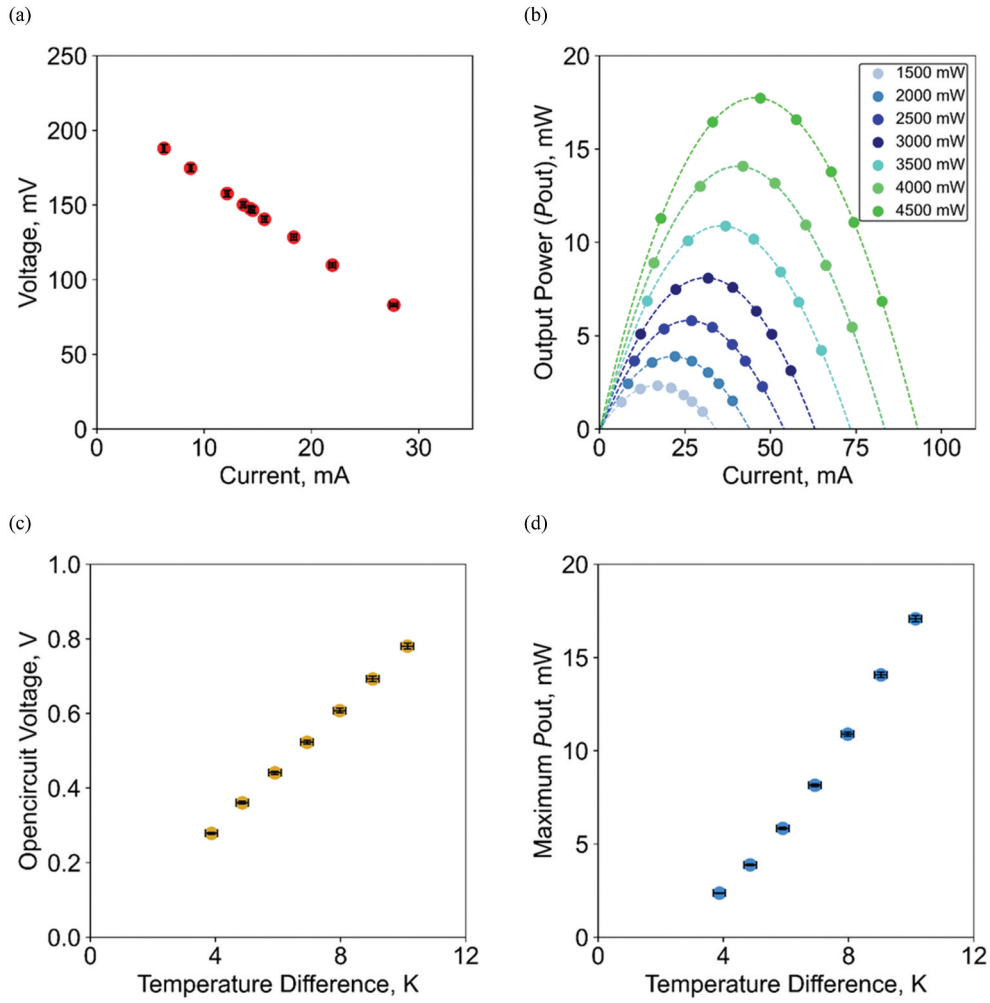


Figure 4. Thermoelectric generation properties obtained by the proposal method. (a) I - V diagram at 1500 mW laser power, (b) the output power for the current at each laser power condition, (c) the open-circuit voltage at each temperature difference, and (d) maximum P_{out} .

$$\frac{u(ZT)}{ZT} = \sqrt{\left(\frac{\partial ZT}{\partial T_h} \delta T_h\right)^2 + \left(\frac{\partial ZT}{\partial T_c} \delta T_c\right)^2 + \left(\frac{\partial ZT}{\partial \eta} \delta \eta\right)^2} \quad (15)$$

ΔT used as the horizontal axis when graphing η and ZT includes the measurement error of each temperature measurement method. The uncertainty of each parameter together with the temperature measurement error for each temperature measurement method is summarized in Table 2.

4.2. Experimental results and discussion

To confirm the validity of the proposed method, we performed a comparative measurement of η and ZT using the conventional method using HFM developed by the National Institute of Advanced Industrial Science and Technology (AIST) [36]. The measurement conditions were adjusted to maintain T_c at 15°C for both the proposed and the conventional methods. Figure 5(a) shows that the η values of the same device obtained by the proposed and conventional methods. Due to the effect of Carnot efficiency, η monotonically

increases as ΔT increases. Importantly, the η values clearly match between these methods within a margin of error. As a possible reason for the slight difference between these methods, it should be noted that the conventional method uses the temperatures of the heat source and sink for T_h and T_c , which may cause an estimation of larger ΔT in the conventional method by including contact thermal resistances. The measurement uncertainty of the proposed method is within 3% at $\Delta T = 4$ K whereas that of the conventional method is 19% at $\Delta T = 5$ K, ensuring the higher reliability of our method even in the low Q_{in} condition.

Figure 5(b) shows the comparison of the ZT values between the proposed and conventional methods and also the catalog values of the same device. As a result of Equation (2) excluding the contribution of the Carnot efficiency from η , the ZT values are almost constant regardless of ΔT in our measurement range. The ZT values for the two methods agree with each other within the error bar. In our method, the standard deviation is less than 2% and the relative error is less than 12% even at low heat flow input, whereas the

Table 2. Uncertainty budget of the evaluation of each parameter at laser power of 1500 mW.

Uncertainty components		Relative standard uncertainty
Proposed method efficiency $u(\eta)/\eta$		3.0%
Proposed method figure of merit $u(ZT)/ZT$		11.4%
Heat flow measurement	Heat transfer coefficient, W/m ² /K	3.4%
	Emissivity of the surface	1.0%
	Laser absorption	1.0%
	Module area, m ²	1.0%
	Laser intensity, W	1.0%
Temperature measurement	Thermography, K (proposed)	1.0°C
	Thermocouple, K (conventional)	0.5°C
	Atmosphere, K (proposed)	1.0°C
	Electrical resistance, Ω	1.0%
Electric power measurement	Voltage measurement, V	1.0%

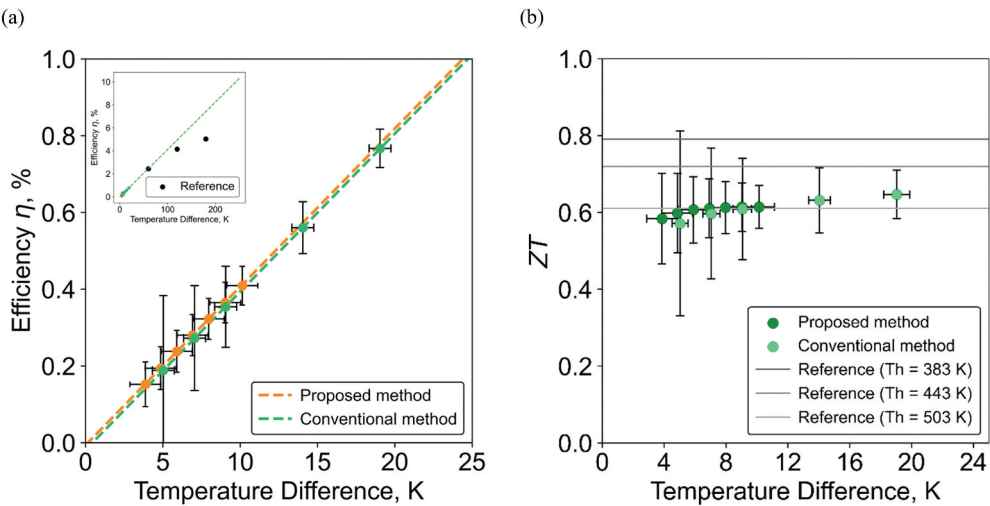


Figure 5. Comparison of the proposed method with the conventional method. (a) The power generation efficiency and (b) ZT value as a function of the temperature difference.

relative error for the conventional method is about 24%. These results indicate that the proposed method is promising for accurate ZT measurements with small temperature differences, which was difficult to achieve with the conventional method.

5. Conclusion

We have developed a simple and accurate measurement method using a laser and thermography to simultaneously evaluate the power generation efficiency η and the device figure of merit ZT of thermoelectric devices. The η and ZT values estimated from the proposed and conventional methods agree with each other within the margin of error. The error analysis reveals that the proposed method shows higher accuracy than the conventional method; the results for the proposed method show an uncertainty of less than 3% for η and less than 12% for ZT with the small temperature difference of 4 K. The proposed method has the versatility to evaluate thermoelectric devices with various dimensions, providing a simpler and more adaptable measurement method. By reducing the complexity of the evaluation process of thermoelectric devices, this method will significantly

contribute to the design and optimization of thermoelectric applications including energy harvesting, where efficiency measurements at small temperature gradients are essential.

Acknowledgments

The authors thank H. Ohshima for technical support.

Disclosure statement

No potential conflict of interest was reported by the author(s).

Funding

This work was supported by ERATO “Magnetic Thermal Management Materials” [No. JPMJER2201] from Japan Science and Technology (JST) and Grants-in-Aid for Scientific Research (KAKENHI) [No. 24K17610] from Japan Society for the Promotion of Science (JSPS).

Data availability statement

The data that support the findings of this study are available from the corresponding authors upon reasonable request.

References

- [1] Borhani S, Hosseini M, Pakrouh R, et al. Performance enhancement of a thermoelectric harvester with a PCM/metal foam composite. *Renew Energy*. 2021;168:1122–1140. doi: [10.1016/j.renene.2021.01.020](#)
- [2] Mu E, Wu Z, Wu Z, et al. A novel self-powering ultrathin TEG device based on micro/nano emitter for radiative cooling. *Nano Energy*. 2019;55:494–500. doi: [10.1016/j.nanoen.2018.10.057](#)
- [3] Rowe D. Thermoelectrics, an environmentally friendly source of electrical power. *Renew Energy*. 1999;16(1–4):1251–1256. doi: [10.1016/S0960-1481\(98\)00512-6](#)
- [4] Shu G, Ma X, Tian H, et al. Configuration optimization of the segmented modules in an exhaust-based thermoelectric generator for engine waste heat recovery. *Energy*. 2018;160:612–624. doi: [10.1016/j.energy.2018.06.175](#)
- [5] Tritt T. Thermoelectric phenomena, materials, and applications. *Annu Rev Mater Res*. 2011;41(1):433–448. doi: [10.1146/annurev-matsci-062910-100453](#)
- [6] Czajczynska D, Krzyzyska R, Jouhara H, et al. Use of pyrolytic gas from waste tire as a fuel: a review. *Energy*. 2017;134:1121–1131. doi: [10.1016/j.energy.2017.05.042](#)
- [7] Kim S, Park S, Kim S, et al. A thermoelectric generator using engine coolant for light-duty internal combustion engine-powered vehicles. *J Electron Mater*. 2011;40(5):812–816. doi: [10.1007/s11664-011-1580-6](#)
- [8] Jung Y, Jeong D, Kang S, et al. Wearable solar thermoelectric generator driven by unprecedentedly high temperature difference. *Nano Energy*. 2017;40:663–672. doi: [10.1016/j.nanoen.2017.08.061](#)
- [9] Ren W, Sun Y, Zhao D, et al. High-performance wearable thermoelectric generator with self-healing, recycling, and lego-like reconssuring capabilities. *Sci Adv*. 2021;7(7):2375–2548. doi: [10.1126/sciadv.abe0586](#)
- [10] Kraemer D, Jie Q, McEnaney K, et al. Concentrating solar thermoelectric generators with a peak efficiency of 7.4. *Nat Energy*. 2016;1(11):1–8. doi: [10.1038/nenergy.2016.153](#)
- [11] Zhang Q, Sun Y, Xu W, et al. Organic thermoelectric materials: emerging green energy materials converting heat to electricity directly and efficiently. *Adv Mater*. 2014;26(40):6829–6851. doi: [10.1002/adma.201305371](#)
- [12] Shittu S, Li GQ, Tang X, et al. Analysis of thermoelectric geometry in a concentrated photovoltaic-thermoelectric under varying weather conditions. *Energy*. 2020;202:117742. doi: [10.1016/j.energy.2020.117742](#)
- [13] Kuroki T, Murai R, Makino K, et al. Research and development for thermoelectric generation technology using waste heat from steelmaking process. *J Electron Mater*. 2015;44(6):2151–2156. doi: [10.1007/s11664-015-3722-8](#)
- [14] Kuroki T, Kabeya K, Makino K, et al. Thermoelectric generation using waste heat in steel works. *J Electron Mater*. 2014;43:2405–2410. doi: [10.1007/s11664-014-3094-5](#)
- [15] Maduabuchi CC, Ejenakevwe KA, Mgbemene CA. Performance optimization and thermodynamic analysis of irreversibility in a contemporary solar thermoelectric generator. *Renew Energy*. 2021;168:1189–1206. doi: [10.1016/j.renene.2020.12.130](#)
- [16] Lim J, Whitacre JF, Fleurial JP, et al. Myung N. Fabrication method for thermoelectric nanodevices. *Adv Mater*. 2005;17(12):1488–1492. doi: [10.1002/adma.200401189](#)
- [17] Xie J, Lee C, Feng HH. Design, fabrication, and characterization of CMOS MEMS-based thermoelectric power generators. *J Microelectromech Syst*. 2010;19(2):317–324. doi: [10.1109/JMEMS.2010.2041035](#)
- [18] Karri M, Thacher E, Helenbrook B. Exhaust energy conversion by thermoelectric generator: two case studies. *Energy Convers Manag*. 2011;52(3):1596–1611. doi: [10.1016/j.enconman.2010.10.013](#)
- [19] Shi Z, Zhang K, Jiang K, et al. Maximizing energy generation: a study of radiative cooling-based thermoelectric power devices. *Energy*. 2020;274:127283. doi: [10.1016/j.energy.2023.127283](#)
- [20] Yuan D, Jiang W, Sha A, et al. Technology method and functional characteristics of road thermoelectric generator system based on Seebeck effect. *Appl Energy*. 2023;331:120459. doi: [10.1016/j.apenergy.2022.120459](#)
- [21] Pawel Z, Przemyslaw B, Byungki R, et al. International round robin test of thermoelectric generator modules. *Materials*. 2022;15(5):1627. doi: [10.3390/ma15051627](#)
- [22] Kanno T, Ando F, Matsuoka Y, et al. Avoiding errors in efficiency measurements of high-performance thermoelectric generator modules: toward best practices for materials researchers. *Mater Today Phys*. 2023;36:101171. doi: [10.1016/j.mtphys.2023.101171](#)
- [23] Rowe DM. Thermoelectrics handbook: macro to nano. Boca Raton: CRC Press; 2006. doi: [10.1201/9781420038903](#)
- [24] Snyder GJ, Snyder AH. Figure of merit ZT of a thermoelectric device defined from materials properties. *Energy Environ Sci*. 2017;10(11):2280–2283. doi: [10.1039/C7EE02007D](#)
- [25] Raju C, Jayachandran B, Takao M. Best practices for evaluating the performance of thermoelectric devices. *Joule*. 2024;20(3):556–562. doi: [10.1016/j.joule.2024.02.009](#)
- [26] Ando F, Tamaki H, Matsuoka Y, et al. Dual-boost thermoelectric power generation in a GeTe/Mg3Sb2-based module. *Mater Today Phys*. 2023;36:101156. doi: [10.1016/j.mtphys.2023.101156](#)
- [27] Périchon S, Lysenko V, Remaki B, et al. Measurement of porous silicon thermal conductivity by micro-Raman scattering. *J Appl Phys*. 1999;86(8):4700–4702. doi: [10.1063/1.371424](#)
- [28] Ishizaki T, Nagano H. “Measurement of 3D thermal diffusivity distribution with lock-in thermography and application for high thermal conductivity CFRPs. *Infrared Phys Technol*. 2019;99:1350–4495. doi: [10.1016/j.infrared.2019.04.023](#)
- [29] Ishizaki T, Nagano H. Microscale mapping of thermal contact resistance using lock-in thermography. *Int J Therm Sci*. 2023;193:108475. doi: [10.1016/j.ijthermalsci.2023.108475](#)
- [30] Fujita R, Alasli A, Yokozeki T, et al. Quantification of early-stage fatigue damage on cross-ply CFRP laminates by lock-in thermographic thermal diffusivity measurement. *Proc SPIE*. 2022;12109:121090F. doi: [10.1007/s10765-025-03523-7](#)
- [31] Ishizaki T, Nagano H. Measurement of three-dimensional anisotropic thermal diffusivities for carbon fiber-reinforced plastics using lock-in thermography. *Int J Thermophys*. 2015;36(10–11):2577–2589. doi: [10.1007/s10765-014-1755-5](#)

- [32] Fujita R, Nagano H. Novel fiber orientation evaluation method for CFRP/CFRTP based on measurement of anisotropic in-plane thermal diffusivity distribution. *Compos Sci Technol.* 2017;140:116–122. doi: [10.1016/j.compscitech.2016.12.006](https://doi.org/10.1016/j.compscitech.2016.12.006)
- [33] Coherent.com [Internet]. Saxonburg (PA): Coherent Corp.; single-stage-thermoelectric-generator-tg12-2.5-ds.pdf; 2022 [cited 2025 Mar 29]. Available from: <https://www.coherent.com/content/dam/coherent/site/en/resources/datasheet/materials/single-stage-thermoelectric-generator-tg12-2.5-ds.pdf>
- [34] Japansensor.co.jp [Internet]. Tokyo: JAPAN SENSOR; [cited 2008 Aug 22]. Available from: <https://www.japansensor.co.jp/manage/wp-content/uploads/2015/03/blackpaint.pdf>
- [35] Alasli A, Fujita R, Nagano H. Thermophysical properties mapping of composites by lock-in thermography: applications on carbon fiber reinforced plastics. *Int J Thermophys.* 2022;43(12):176. doi: [10.1007/s10765-022-03109-7](https://doi.org/10.1007/s10765-022-03109-7)
- [36] Ohta M, Jood P, Murata M, et al. An integrated approach to thermoelectrics: combining phonon dynamics, nanoengineering, novel materials development, module fabrication, and metrology. *Adv Energy Mater.* 2019;9(23):1801304. doi: [10.1002/aenm.201801304](https://doi.org/10.1002/aenm.201801304)